Supplementary Data

Structural basis for RNA recognition by NusB and NusE in the initiation of transcription antitermination

Jason R. Stagno[1], Amanda S. Altieri[2], Mikhail Bubunenko[3,4], Sergey G. Tarasov[2], Jess Li[2], Donald L. Court[3], R. Andrew Byrd[2], and Xinhua Ji[1,*]

[1]Macromolecular Crystallography Laboratory, [2]Structural Biophysics Laboratory, and [3]Gene Regulation and Chromosome Biology Laboratory, National Cancer Institute, Frederick, MD 21702, USA and [4]Basic Research Program, SAIC-Frederick, Inc., National Cancer Institute, Frederick, MD 21702, USA

*To whom correspondence should be addressed. Tel: (301) 846-5035; Fax: (301) 846-6073; E-mail: jix@mail.nih.gov

SUPPLEMENTARY MATERIALS AND METHODS

Cloning, coexpression, and purification of AaNusB-NusE

*Aa*NusB was prepared as described (1). To coexpress the *Aa*NusB-NusE complex, genes encoding *Aa*NusE (residues 47-68 replaced with a single Ser) and *Aa*NusB were cloned into suitable donor vectors, followed by multi-site recombination into a tagless destination vector (pDEST42) using Gateway® cloning technology (Invitrogen, Carlsbad, CA). *Aa*NusE was cloned in front of *Aa*NusB, each preceded by a ribosome-binding site.

BL21(DE3) RIL (Stratagene, La Jolla, CA) cells were transformed with plasmid by electroporation, and transformants were grown overnight in Lysogeny Broth (LB) medium containing 100 μg/ml ampicillin (Amp_{100}). Overnight culture was used to inoculate 1 L volumes of LB/Amp_{100} and the cells were grown to an optical density of 0.8-1.0 at 600 nm, upon which the temperature was reduced to 18 ˚C, and expression induced with 1 mM IPTG. Cells were harvested approximately 20 hours post-induction.

Cell pellets were resuspended (10% w/v) in a lysis buffer containing 25 mM Bis-Tris pH 6.2, 1 mM EDTA, and a protease inhibitor cocktail (Roche Molecular Biochemicals, Indianapolis, IN). The cells were lysed at 10,000 psi using an APV-1000 homogenizer (Invensys, Roholmsvej, Denmark) and clarified by centrifugation at 15,000 g for 60 minutes. The soluble fraction was incubated for 30 minutes at 90 ˚C and clarified again by centrifugation at 15,000 g for 60 minutes. The sample was purified by ion-exchange chromatography using SP Sepharose (HiTrap SP FF, GE Healthcare, Piscataway, NJ) in the lysis buffer and eluted using a linear gradient (0-1 M) of NaCl. Fractions were analyzed by SDS-PAGE and pure fractions were pooled and concentrated to ~500 μM. *Aa*BoxA and dilution buffer were added to give final concentrations of 425 μM protein, 500 μM RNA. The sample was vortexed briefly followed by incubation at 70 ˚C for 15 minutes. The sample was then cooled slowly back to room temperature (~1 hour), centrifuged to remove particulate matter, and used immediately for crystallization.

NMR experiments for melting point determination of *Aa* and *Ec rrn* BoxA RNAs

The duplex form of RNA is stabilized by several hydrogen bonds from base to base across separate strands. Hydrogen bonding of the guanosine H_{N3} and uracil H_{N1} in these base pairs slows down the exchange rate with the solvent such that these protons are observable by NMR. The unique magnetic environment of these nuclei also gives them markedly downfield chemical shifts, which are readily observable in homonuclear spectra (12.4 ppm and 13.1 ppm for G and U, respectively). One-dimensional NMR spectra using a double-echo (2) pulse sequence were collected for *Aa* 16S *rrn* BoxA (5'-GGCUCCUUGGCA-3', *Aa*BoxA) and *Ec rrn* BoxA (5'-UGCUCUUUAACA-3', *Ec*BoxA) on a Varian Inova spectrometer at 800 MHz equipped with a ChiliProbe. The RNA samples were 0.5 to 1 mM in 50 mM Tris or phosphate buffer with 50 mM NaCl and 1 mM EDTA at pH 6.5. Spectra were collected at the following temperatures: 25, 30, 32.5 and 35 °C. The far downfield region was inspected for the presence of peaks which indicate self-hybridization of the RNA. The *Ec*BoxA showed no tendency to hybridize under any temperature as no downfield peaks were observed. The *Aa*BoxA showed 4 downfield peaks in the 25 °C spectrum at 13.1, 12.8, 11.2, and 10.2 ppm indicative of at least 4 base pairs. These data are consistent with the duplexed RNA observed in the *Aa*NusB-NusE-dsRNA crystal

structure. Upon increasing the temperature, the peaks in the NMR spectrum decreased until they were no longer observable at and above 32.5° C. The crystallization temperature was then set to 37 °C to ensure the single-stranded form of *Aa*BoxA was the dominant form of RNA during the crystallization process, resulting in the *Aa*NusB-NusE-BoxA crystal structure.

Crystallization and structure determination

Crystals of *Aa*NusB-NusE-BoxA were grown at 37 ˚C in sitting drops containing 0.4 μl protein solution (425 μM *Aa*NusB-NusE and 500 μM 12-mer *Aa*BoxA RNA in 25 mM Bis-Tris pH 6.2, 300 mM NaCl, and 1 mM EDTA) and 0.2 μl well solution (25% PEG-8000 in 0.1 M sodium acetate pH 4.6). A crystal of *Aa*NusB-NusE-BoxA was soaked in a cryoprotectant solution containing 80% (v/v) well solution and 20% (v/v) PEG-200 and flash-frozen in liquid nitrogen.

Crystals of *Aa*NusB-NusE-dsRNA were grown at room temperature in sitting drops containing 0.4 μl protein solution (425 μM *Aa*NusB-NusE and 500 μM 12-mer *Aa*BoxA RNA in 25 mM Bis-Tris pH 6.2, 300 mM NaCl, and 1 mM EDTA) and 0.2 μl well solution (0.2 M diammonium phosphate and 20% PEG-3350). A crystal of *Aa*NusB-NusE-dsRNA was soaked in a cryoprotectant solution containing 80% (v/v) well solution and 20% (v/v) PEG-200, and flash-frozen in liquid nitrogen.

All data were collected at the Advanced Photon Source and processed with HKL3000 (3). Molecular replacements were performed using Phaser (4). The *Aa*NusB-NusE-dsRNA structure was solved using *Ec*NusB-NusE (PDB ID: 3D3B) as a search model and the *Aa*NusB-NusE-BoxA structure was solved using *Aa*NusB-NusE-dsRNA as a search model. Solvent and ligand atoms were excluded from the search models. Model building and refinement were carried out using the programs COOT (5) and PHENIX (6), respectively. NCS restraints were applied in the refinement of *Aa*NusB-NusE-dsRNA, and TLS parameters were used in the refinements of both structures. The structures were validated using the programs WHAT IF (7) and PROCHECK (8). All figures were generated using PyMol (9). Data, refinement statistics, and other structural information are summarized in Table 1.

***Ec*NusB cloning and overexpression**

*Ec*NusB proteins were cloned, expressed, and purified as previously described (1,10). The *EcnusB-C12A/D118N* mutant was made by introducing a pair of complementary oligomers bearing the mismatch at D118 for Asn. Mutagenesis was performed with the QuickChange Mutagenesis Kit (Stratagene, La Jolla, CA) using the *nusB-C12A*/pET3a clone. The *EcnusB-C12A/Y18D* mutation was introduced by a pair of complementary oligomers bearing the mismatch at Y18 for Asp using QuickChange Mutagenesis Kit (Stratagene, La Jolla, CA) in the *nusB-C12A*/pET3a clone. Sub-cloning of the *EcnusB-F122D* gene into the pET3a vector was achieved by PCR using the same oligomers for sub-cloning of wild-type (wt) *EcnusB*. PCR was based on the pAB27 clone, which carries the F122D mutation. Positive clones were identified by DNA sequencing, then transformed and expressed in BL21 pLysS cells (Invitrogen, Carlsbad, CA).

Functional assay for *Aa*NusB complementation in *E. coli*

Standard bacteriological media and techniques were used to cultivate cells (11). We tested whether *Aa*NusB is functional in *E. coli* by measuring how well its *trans*-expression complements the growth defects of the *EcΔnusB* cells. The entire *nusB* ORF (open reading frame) was deleted from the *E. coli* chromosome by recombineering as described (12). As a consequence of the *EcnusB* deletion, the *EcΔnusB* cells were cold sensitive at temperatures lower than 30 ˚C and slow-growing at the normal temperature of 37 ˚C. The *AanusB* was cloned into pET11c as described (1) to create pKM772. The *EcnusB* was cloned into pPCR-Amp from the *E. coli* chromosome by recombineering (12) to create pAB47. *Ec*NusB was expressed from pAB47 without IPTG induction due to the leaky expression from P_{lac}. *Aa*NusB was expressed from pKM772 by constitutive expression from P_{bla}, which is positioned in the same orientation as *nusB* in pKM772.

To assess the functional activity of *Aa*NusB in *E. coli*, the *EcΔnusB* W3110 cells were transformed with plasmids expressing pAB47, pKM772, or the pET vector control. The recombinant colonies were selected on L plates with Amp_{100} at 37 ˚C. Cells from each type of recombinant colony were streaked side-by-side on four sector L plates with Amp_{100} and incubated at 30, 37, or 42 ˚C for 1-2 days.

To assay for the NusB requirement in the growth of phage λ, the *EcΔnusB* cells containing the *Aa*NusB, *Ec*NusB, or control plasmids, were grown overnight at 37 ˚C in LB/Amp_{100}. The overnight cultures were diluted 1:10, incubated for 2 hours in tryptone broth (TB) with 10 mM $MgSO_4$ and Amp_{50}, mixed with TB top agar, and spread over TB agar plates containing Amp_{50}. Serial phage dilutions were spotted and the plates were incubated at 42 ˚C to observe the formation of λ plaques. In contrast to wt phage λ, the λ*nin5* mutant does not require NusB for phage growth and was thus used as a positive control for plaque formation.

***Ec*NusB-C12A for NMR and biophysical studies is analogous to the wild type**

The only cysteine residue in *Ec*NusB, C12, was mutated to an Ala to prevent dimerization of the natively monomeric *Ec*NusB protein. The *Ec*NusB-C12A mutant protein (hereafter referred to as C12A) and wt *Ec*NusB exhibit comparable α-helical content based on circular dichroism spectra (10). In addition, the majority of the resonances in the ^{1}H-^{15}N HSQC spectrum of C12A are superimposable with those in the wt *Ec*NusB spectrum. The few observed chemical shift differences are less than 0.2 ppm and are exhibited only for residues within a few angstroms of the site of the mutation, and are assigned by inspection: A13, Q15, A16, L17, V30, L35, E37, D42 and R49. The C12A mutation does not affect cellular function, as it is able to complement a cold-sensitive *ΔnusB* strain of *E. coli* for all known functions of *Ec*NusB, including phage λ growth (Figure 3). The C12A protein is an acceptable analog to wt *Ec*NusB (Supplementary Table S2) and is used in the majority of the biophysical experiments on *Ec*NusB reported here.

***Ec*NusB-RNA complexes for NMR studies**

*Ec*BoxA RNA was synthesized and gel purified by Trilink BioTechnologies (San Diego, CA). The RNA sequences used are as follows: *Ec*BoxA (5´-UGC UCU UUA ACA-3´), λBoxA (5´-CGC UCU UAC ACA-3´), and *Ec*BoxA-BoxB (5´-GCC GCG CCG CUG AGA AAA AGC GAA GCG GCA CUG CUC UUU A-3´). Purified *Ec*NusB proteins were dialyzed into 50 mM

potassium phosphate buffer pH 6.5, 20 mM EDTA, 20 mM KCl, and 100 μM TCEP (for F122D only). Lyophilized RNA samples were dissolved to desired concentration in the above buffer. The *Ec*NusB-RNA complex samples for NMR were prepared by adding RNA to protein in a ratio of 1.2:1 (RNA:protein) at a protein concentration of ~20 μM, then concentrating using an Amicon stirred cell with a 1,000 MWCO membrane to a final concentration of 200-300 μM. SuperaseIn (Ambion, Inc. Austin, TX) was added to each sample to prevent RNA degradation.

NMR assignments for *Ec*NusB-BoxA

Many resonances in the ^{1}H-^{15}N HSQC spectrum of *Ec*NusB shifted dramatically upon binding of *Ec*BoxA RNA, which required complete reassignment of the protein resonances (Supplementary Figure S3). NMR spectra were collected on Varian Inova spectrometers at either 600 or 800 MHz equipped with ChiliProbes. Sequential backbone assignments were made using standard triple resonance pulse sequences (13). Data were processed and analyzed using NMRPipe (14) and CCPNMR (15) and scripts therein. Sequential backbone and side-chain assignments were complete for ~95% of the protein. The following *Ec*NusB residues gave no detectable H^N resonances: M1-K2, A5, R7, and S119-F122. The amide resonances for residues S119-F122 are readily observed in free *Ec*NusB. The side-chains of H120 and F122 are observable and not exchange-broadened in the *Ec*BoxA-bound *Ec*NusB HSQC spectra. The H^N atoms for S119-F122 of the *Ec*NusB-BoxA complex exhibit intermediate exchange, perhaps reflecting weakened α-helical backbone interactions at the N-terminus of helix α7 upon *Ec*BoxA binding. Due to the importance of F122 in BoxA binding, as well as the largest Δδ observed near F122, residues S119-K121 were included in the chemical shift map, but colored in gray (Figure 2D).

The 2D ^{1}H-^{15}N Heteronuclear Single Quantum Correlation (HSQC) spectra were collected using ^{15}N-labeled NusB protein and non-isotopically labeled RNA. The Δδ were calculated from the peaks in these spectra as: $\Delta\delta\ (ppm) = [(\Delta\nu^{1}H)^2 + 0.2(\Delta\nu^{15}N)^2]^{½}$ where $\Delta\nu^{1}H$ is the difference in the ^{1}H resonance chemical shifts and $\Delta\nu^{15}N$ is the difference in the ^{15}N resonance chemical shifts.

Ultracentrifugation and Gel Filtration of *Ec*NusB-BoxA

*Ec*NusB and *Ec*BoxA form a 1:1 complex based on gel filtration and sedimentation equilibrium centrifugation, with apparent molecular masses of 17.5 kDa and 20.0 kDa for *Ec*NusB and the *Ec*NusB-BoxA complex, respectively. For the *Ec*NusB-BoxA complex, *Ec*NusB was mixed with a several-fold molar excess of *Ec*BoxA RNA and isolated by analytical gel filtration using a Superdex 75 column (1 cm x 30 cm, GE Healthcare, Piscataway, NJ) equilibrated with 50 mM potassium phosphate buffer, pH 6.8, 50 mM NaCl, and 1mM DTT (buffer A). The sample size was 0.20 ml and 0.5 ml fractions were collected. Analytical ultracentrifugation (AUC) was performed at 25,000 rpm, 20 °C, using a Beckman XL-1 Optima analytical ultracentrifuge (Beckman Coulter, Inc., Brea, CA) with an An-60 Ti rotor and standard double-sector centerpiece cells. Protein and *Ec*BoxA were in buffer A. Solvent density was calculated according to reference (16). The partial specific volume of the protein (0.744) was calculated from the predicted amino acid composition (17). Centrifugation data was analyzed using the Beckman-Origin software. Direct sedimentation equilibrium analysis was complicated by unbound *Ec*BoxA RNA, so an *Ec*NusB-BoxA mixture was fractionated by gel filtration and a pure complex was isolated (A_{254} : A_{290} = 1.4; *cf* protein alone = 0.55). The molecular weight

estimates from AUC suggested a less than 1:1 (*Ec*NusB : *Ec*BoxA) molar ratio - the best estimates are a ratio of 1:0.5. However, a loss of RNA due to equilibrium binding during gel filtration could account for this.

Isothermal Titration Calorimetry (ITC) Experiments

The protein-RNA interaction studies were performed using a VP-ITC Microcalorimeter (MicroCal LLC, Northampton, MA) at 25 °C. The typical experiment included injections of 25 aliquots (10 μL each) of 0.1 – 0.2 mM RNA into a 0.01-0.02 mM protein solution in the ITC cell (volume ~1.4 ml). An additional set of injections was run as a reference experiment, using buffer in the cell in place of the protein. The reference data were subtracted from the main experimental titration data. The integrated heat-of-interaction values were fit using the Origin 7.0-based ITC data analysis software (MicroCal). The data fit best to a single-binding-site model, from which binding affinity, stoichiometry, ΔH, and ΔS values were calculated. The ITC experiment for the single-stranded form of *Aa*BoxA RNA was conducted at 35 °C with *Aa*BoxA in the cell at 0.02 mM concentration, and 0.20 mM *Aa*NusB protein as the titrant.

SUPPLEMENTARY DISCUSSION

Implications for RNA Binding to NusB-NusE in *Ec rrnG* Antitermination

Though antitermination has been best characterized in the phage λ system, it is relevant to discuss our results in the context of work on related antitermination systems. The *rrnG* transcriptional antitermination system contains many of the same protein and RNA components as the phage λ system (18-20). The sequence and/or fold of the BoxA and BoxB components are similar between the two systems; however, the order of RNA components is opposite and the spacer between them in *rrnG* contains only two bases (Figure S7A). The two crystal structures reported in this study, *Aa*NusB-NusE-BoxA and *Aa*NusB-NusE-dsRNA, are superimposed in Figure S7B. The proximity of the BoxA and dsRNA-binding sites to each other serves as a focal point for this discussion.

In *rrnG* antitermination, NusB and BoxA are required, since activity is lost upon mutation of either; in contrast, the BoxB component is not essential, since a *boxB* deletion mutant maintains antitermination activity (19-21). When BoxB is present, however, it plays some role as two single mutations in BoxB have been shown to impair antitermination even in the presence of wild-type BoxA (19). These mutations, *boxB(C2A) and boxB(C3A),* would each disrupt a G-C base pair in the stem region of BoxB (Figure S7A). If BoxB interacts at the nearby dsRNA-binding site on the NusB-NusE complex, these mutations would disrupt the dsRNA feature that is recognized by the protein heterodimer. The exact mechanism of how BoxB mutations affect antitermination in *rrnG* is not clear, though the results of Berg *et al*. (19) imply that the secondary structure of RNA does play a role. The presence of BoxB-like sequences in *rrn* terminator-like sequences of many other bacteria (19) and in all seven *E. coli* operons imply that the BoxB feature is associated with BoxA-mediated antitermination in many systems. Though not always required, dsRNA binding to NusB-NusE could be utilized as an interaction point for dsRNA features under certain conditions and for particular systems of transcriptional regulation.

SUPPLEMENTARY REFERENCES

1. Das, R., Loss, S., Li, J., Waugh, D.S., Tarasov, S., Wingfield, P.T., Byrd, R.A. and Altieri, A.S. (2008) Structural biophysics of the NusB:NusE antitermination complex. *J. Mol. Biol.*, **376**, 705-720.
2. Hwang, T.-L. and Shaka, A.J. (1995) Water suppression that works. Excitation sculpting using arbitrary waveforms and pulsed field gradients. *J. Magn. Reson., Series A*, **112**, 275-279.
3. Otwinowski, Z. and Minor, W. (1997) Processing of X-ray diffraction data collected in oscillation mode. *Methods Enzymol.*, **276**, 307-326.
4. McCoy, A.J., Grosse-Kunstleve, R. W., Adams, P. D., Winn, M. D., Storoni, L.C. & Read R.J. . (2007) Phaser crystallographic software. *J. Appl. Crystallogr.*, **40**, 658-674.
5. Emsley, P. and Cowtan, K. (2004) Coot: model-building tools for molecular graphics. *Acta Crystallogr. D*, **60**, 2126-2132.
6. Adams, P.D., Grosse-Kunstleve, R.W., Hung, L.W., Ioerger, T.R., McCoy, A.J., Moriarty, N.W., Read, R.J., Sacchettini, J.C., Sauter, N.K. and Terwilliger, T.C. (2002) PHENIX: building new software for automated crystallographic structure determination. *Acta Crystallogr. D*, **58**, 1948-1954.
7. Vriend, G. (1990) WHAT IF: a molecular modeling and drug design program. *J. Mol. Graph.*, **8**, 52-56, 29.
8. Laskowski, R.A., MacArthur, M.W., Moss, D.S. and Thornton, J.M. (1993) PROCHECK: a program to check stereochemical quality of protein structures. *J. Appl. Crystallogr.*, **26**, 283-291.
9. DeLano, W.L. (2002). Delano Scientific, San Carlos, CA.
10. Altieri, A.S., Mazzulla, M.J., Zhou, H.J., Costantino, N., Court, D.L. and Byrd, R.A. (1997) Sequential assignments and secondary structure of the RNA-binding transcriptional regulator NusB. *FEBS Lett.*, **415**, 221-226.
11. Miller, J.H. (1972) *Experiments in Molecular Genetics*. Cold Spring Harbor Laboratory, Cold Spring Harbor, NY.
12. Bubunenko, M., Baker, T. and Court, D.L. (2007) Essentiality of ribosomal and transcription antitermination proteins analyzed by systematic gene replacement in *Escherichia coli*. *J. Bacteriol.*, **189**, 2844-2853.
13. Sattler, M., Schleucher, J. and Griesinger, C. (1999) Heteronuclear multidimensional NMR experiments for the structure determination of proteins in solution employing pulsed field gradients. *Prog Nucl Mag Res Sp*, **34**, 93-158.
14. Delaglio, F., Grzesiek, S., Vuister, G.W., Zhu, G., Pfeifer, J. and Bax, A. (1995) NMRPipe - a multidimensional spectral processing system based on unix pipes. *J. Biomol. NMR*, **6**, 277-293.
15. Vranken, W.F., Boucher, W., Stevens, T.J., Fogh, R.H., Pajon, A., Llinas, M., Ulrich, E.L., Markley, J.L., Ionides, J. and Laue, E.D. (2005) The CCPN data model for NMR spectroscopy: development of a software pipeline. *Proteins: Struct. Funct. Genet.*, **59**, 687-696.
16. Laue, T.M., Shah, B.D., Ridgeway, T.M. and Pelletier, S.L. (1992) *Computer-aided interpretation of analytical sedimentation data for proteins*. In Harding, S. E., Rowe, A. J. and Horton, J. C. (eds.), *Analytical ultracentrifugation in biochemistry and polymer science*. Royal Society of Chemistry, Cambridge, United Kingdom, pp. 94-115.

17. Cohn, E.J. and Edsall, J.T. (1943) *Proteins, Amino Acids and Peptides*. Van Nostrand-Reinhold, Princeton, NJ.
18. Friedman, D.I. and Olson, E.R. (1983) Evidence that a nucleotide sequence, "boxA," is involved in the action of the NusA protein. *Cell*, **34**, 143-149.
19. Berg, K.L., Squires, C. and Squires, C.L. (1989) Ribosomal RNA operon anti-termination. Function of leader and spacer region box B-box A sequences and their conservation in diverse micro-organisms. *J. Mol. Biol.*, **209**, 345-358.
20. Squires, C.L., Greenblatt, J., Li, J., Condon, C. and Squires, C.L. (1993) Ribosomal RNA antitermination in vitro: requirement for Nus factors and one or more unidentified cellular components. *Proc. Natl. Acad. Sci. USA*, **90**, 970-974.
21. Nodwell, J.R. and Greenblatt, J. (1993) Recognition of boxA antiterminator RNA by the *E. coli* antitermination factors NusB and ribosomal protein S10. *Cell*, **72**, 261-268.
22. Altieri, A.S., Mazzulla, M.J., Horita, D.A., Coats, R.H., Wingfield, P.T., Das, A., Court, D.L. and Byrd, R.A. (2000) The structure of the transcriptional antiterminator NusB from *Escherichia coli*. *Nat. Struct. Biol.*, **7**, 470-474.

SUPPLEMENTARY TABLE S1

Table S1. *In vivo* functional properties of *Ec*NusB mutants

*Ec*NusB allele	*E. coli* growth [a]	λ growth at 37 °C [b]
nusB^{+}	normal	normal
ΔnusB	cold-sensitive	poor
nusB-F122D	cold-sensitive	poor
*nusB*5(Y18D)	normal	poor
nusB101(D118N)	normal	normal [c]

[a] Cold-sensitive growth indicates that cells form colonies on L plates at 37 °C, but not at 30 °C. Normal indicates that colonies form at both temperatures.

[b] Normal λ growth implies efficient plaque formation; poor growth indicates an inefficiency in plaque formation (10^{-4}).

[c] *nusB101* rescues λ growth defects caused by mutations *nusA1* and *nusE71*.

SUPPLEMENTARY TABLE S2

Table S2. Isothermal titration calorimetry of NusB with BoxA RNA sequences [a]

	RNA 5´ 3´	K_d (μM)	N	ΔH (kcal/mol)	ΔS (cal/mol/deg)
***Ec*NusB**					
*Ec*BoxA	UGCUCUUUAACA	2.1 (0.3)	0.9	-1.27 (0.03)	-17.4
rev *Ec*BoxA	ACAAUUUCUCGU	*n.b.*	-	-	-
random	GUAGAGGGCCAC	*n.b.*	-	-	-
***Ec*C12A**					
*Ec*BoxA	UGCUCUUUAACA	1.6 (0.2)	0.83	-1.45 (0.01)	-22.8
λnutR BoxA	CGCUCUUACACA	2.8 (0.3)	0.63	-1.55 (0.04)	-27.6
rev *Ec*BoxA	ACAAUUUCUCGU	*n.b.*	-	-	-
***Ec*D118N [b], C12A**					
*Ec*BoxA	UGCUCUUUAACA	0.22 (0.02)	0.67	-1.62 (0.02)	-24.8
λnutR BoxA	CGCUCUUACACA	0.74 (0.16)	0.98	-1.67 (0.06)	-27.9
rev *Ec*BoxA	ACAAUUUCUCGU	*n.b.*	-	-	-
***Ec*Y18D [c], C12A**					
*Ec*BoxA	UGCUCUUUAACA	0.4 (0.2)	0.60	-1.80 (0.35)	-31.8
rev *Ec*BoxA	ACAAUUUCUCGU	*n.b.*	-	-	-
***Ec*F122D**					
*Ec*BoxA [d]	UGCUCUUUAACA	*n.b.*	-	-	-
rev *Ec*BoxA	ACAAUUUCUCGU	*n.b.*	-	-	-
***Aa*NusB**					
*Aa*BoxA	GGCUCCUUGGCA	0.016 (0.003)	0.82	49.5 (0.14)	202
*Aa*BoxA (35 °C) [e]	GGCUCCUUGGCA	0.067 (0.005)	1.0	9.08 (0.08)	62.3
*Ec*BoxA	UGCUCUUUAACA	4.3 (0.3)	0.90	-6.55 (0.42)	2.59
λnutR BoxA	CGCUCUUACACA	*n.b.*	-	-	-

[a] No binding detected is represented as *n.b.*
[b] *nusB101* equivalent.
[c] *nusB5* equivalent.
[d] F122D showed a slight binding interaction at higher concentrations and in the presence of an excess of *Ec*BoxA, as observed by ^{1}H-^{15}N HSQC spectra (Supplementary Figure S4B).
[e] All other experiments performed at 25 °C.

SUPPLEMENTARY FIGURE S1

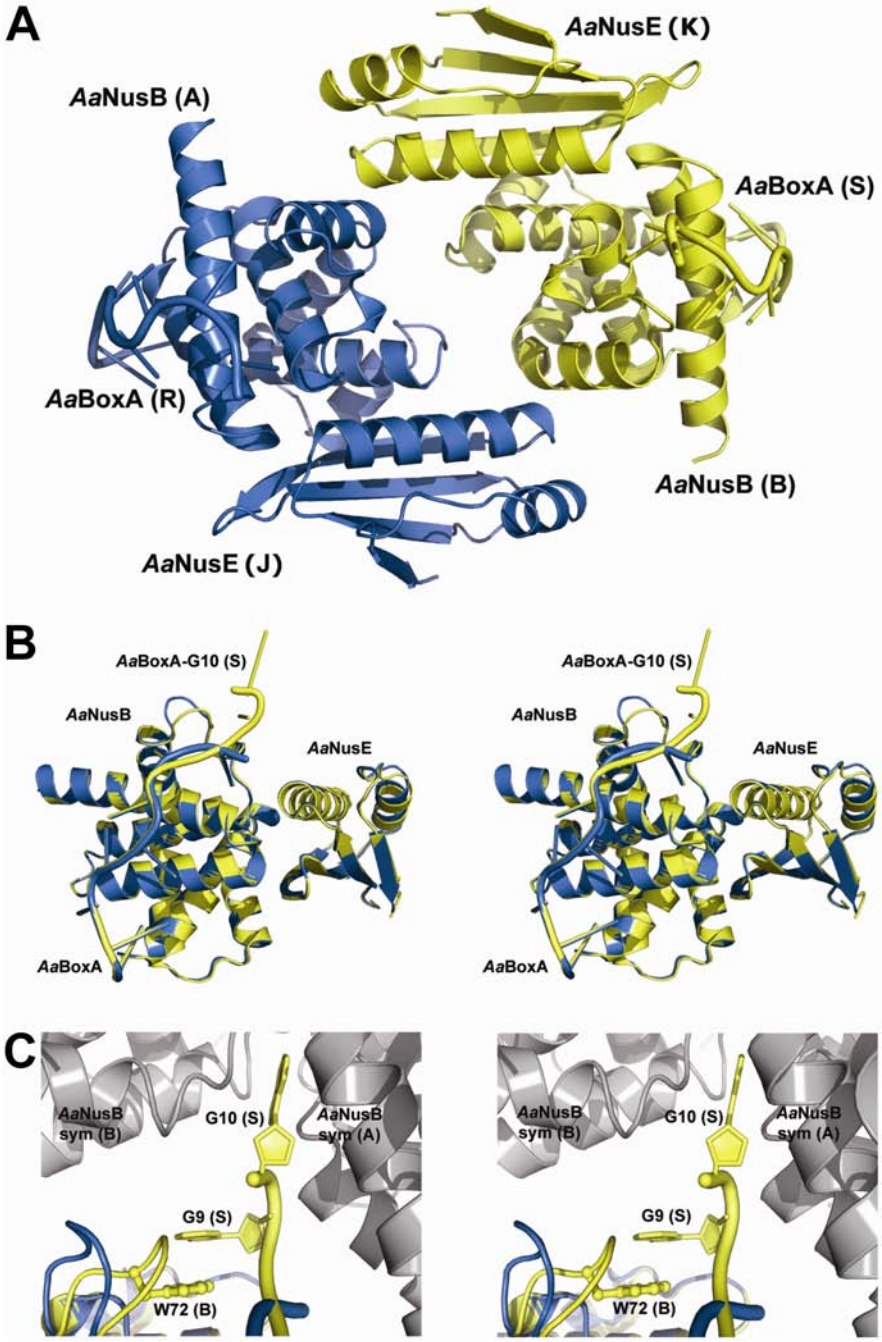

Figure S1. Analysis of the crystal structure of *Aa*NusB-NusE-BoxA. (**A**) Overall structure of the asymmetric unit of *Aa*NusB-NusE-BoxA, viewed along the non-crystallographic 2-fold axis of symmetry, which is generated by dimerization of two ternary complexes (blue and yellow). (**B**) Superposition of the two ternary complexes (blue: chains A, J, R; yellow: chains B, K, S) in stereo. The major differences are observed at the 3´ end of *Aa*BoxA. (**C**) Close-up view of *Aa*BoxA-G10 (chain S) in stereo, which is wedged between two symmetry-related molecules of *Aa*NusB (gray).

SUPPLEMENTARY FIGURE S2

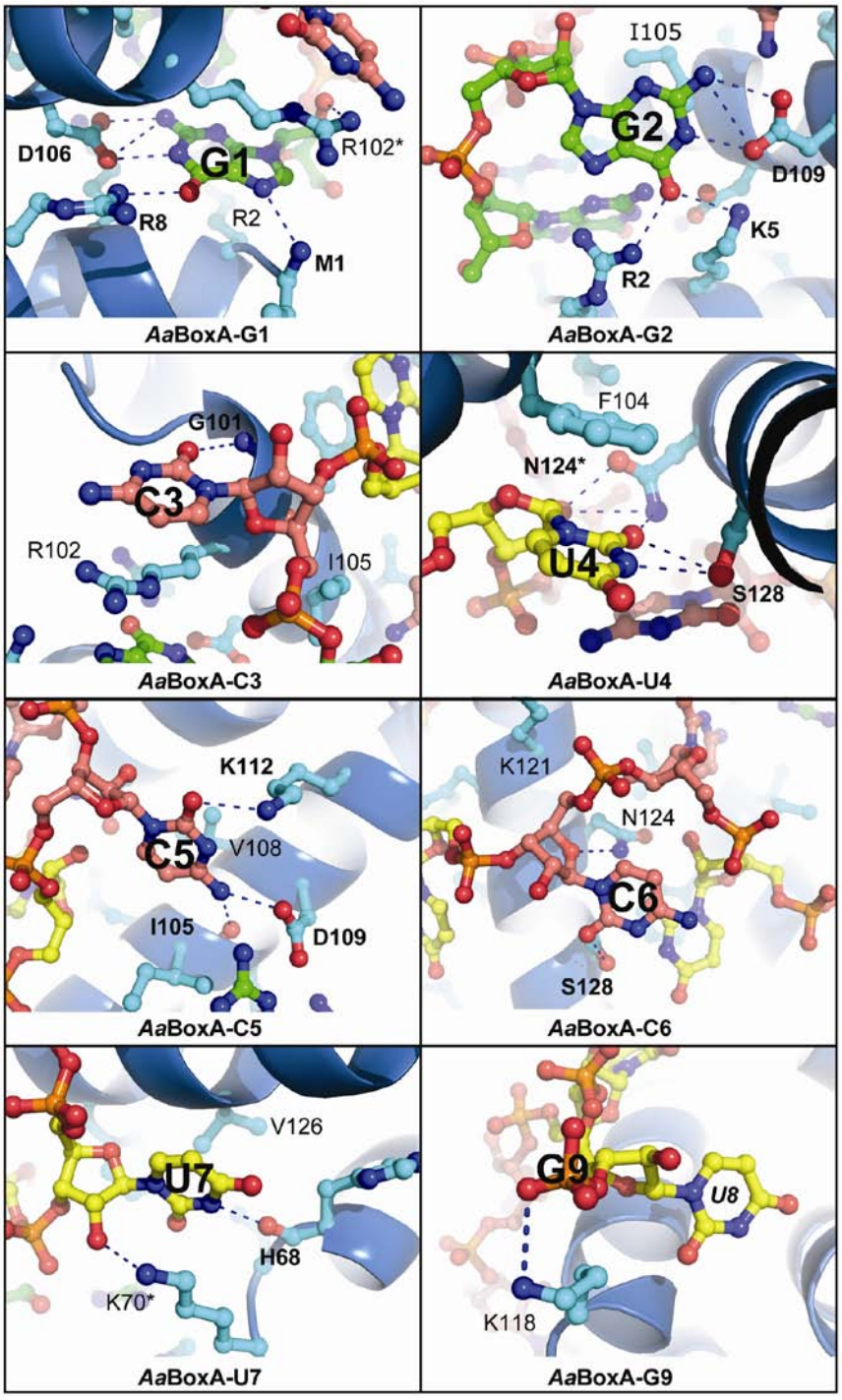

Figure S2. Detailed interactions of *Aa*NusB with *Aa*BoxA in the *Aa*NusB-NusE-BoxA structure. RNA-protein interactions are illustrated for *Aa*BoxA nucleotides 1-7 and the 5' phosphate group of 9 as observed in the crystal structure of *Aa*NusB-NusE-BoxA. The RNA bases are color-coded as in Figure 2.

SUPPLEMENTARY FIGURE S3

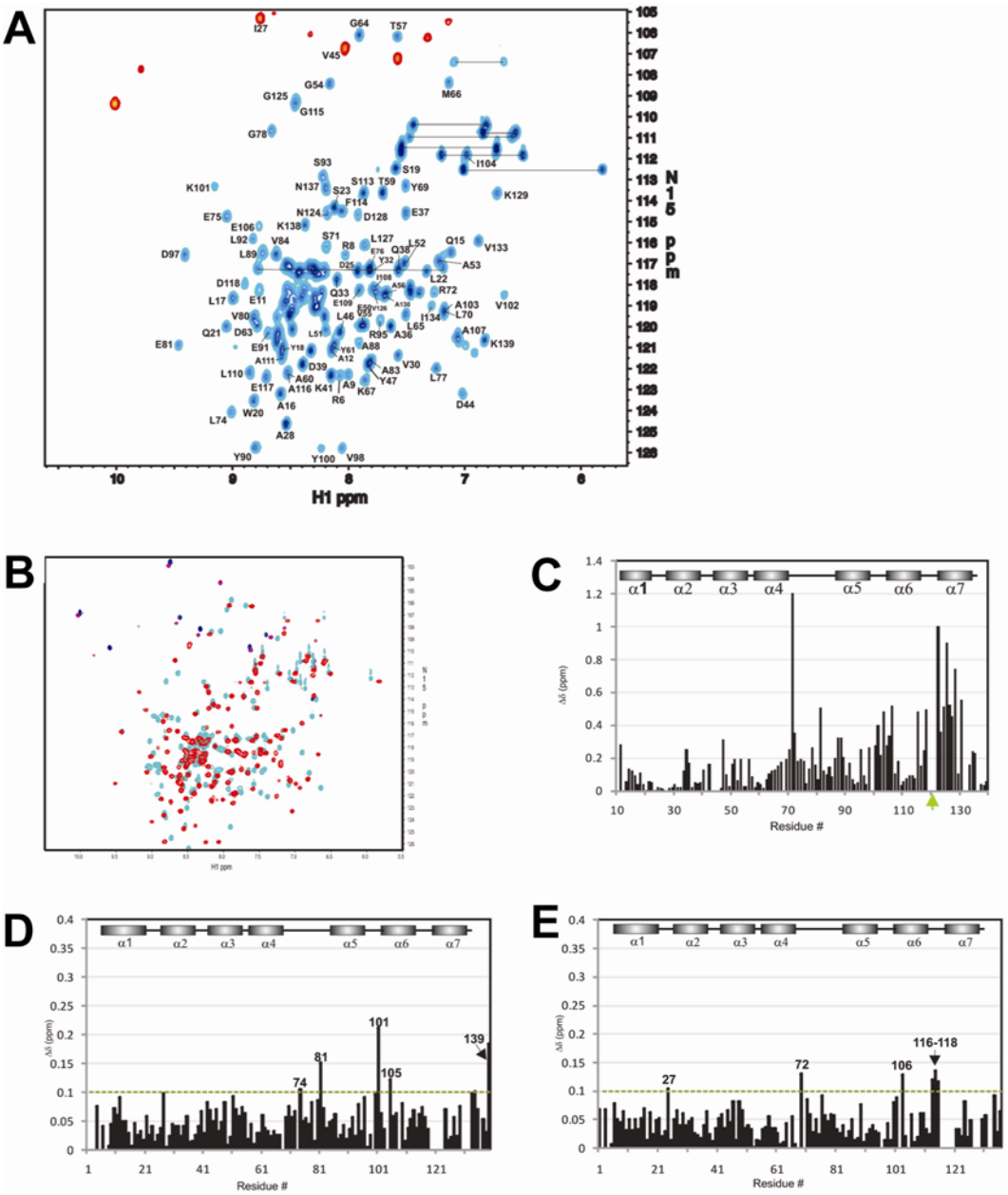

Figure S3. NMR data for the *Ec*BoxA-binding site of *Ec*NusB. (**A**) HSQC spectrum of *Ec*NusB bound to *Ec*BoxA RNA with labeled resonance assignments. (**B**) Overlay of HSQC spectra of free *Ec*NusB (green contours) and *Ec*NusB-BoxA (red contours). (**C**) Observed Δδ of NH resonances between free *Ec*NusB and the *Ec*NusB-BoxA complex. The green arrows note the location of resonances S119-H120 that are exchange-broadened in the complex. (**D**) Observed Δδ by residue number of NH resonances for *Ec*NusB-D118N-BoxA *versus* *Ec*NusB-D118N-BoxA-U1C. (**E**) Observed Δδ by residue number of NH resonances for *Ec*NusB-D118N-BoxA *versus* *Ec*NusB-D118N-BoxA-A9C.

SUPPLEMENTARY FIGURE S4

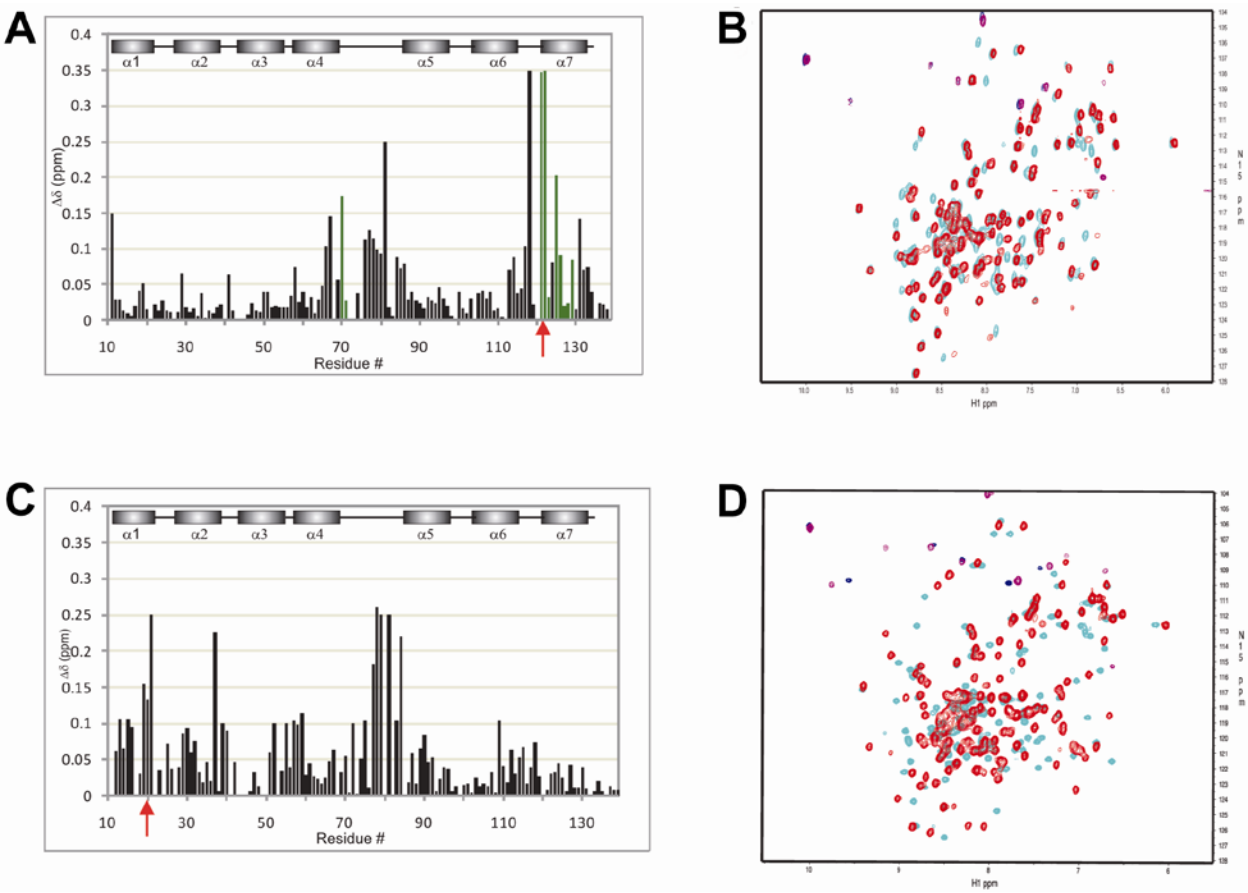

Figure S4. Chemical shift effects of *Ec*NusB mutations**.** (**A**) Observed Δδ in ppm of NH resonances of the free proteins for *Ec*NusB-F122D relative to wt *Ec*NusB (10). Most of the shift effects are localized near residue F122 in the folded protein. The bars shown in green indicate residues affected by the absence of ring current effects in the mutant protein. The red arrows indicate the sites of mutation. (**B**) HSQC spectral overlay of *Ec*NusB-F122D and *Ec*NusB-F122D with an excess of *Ec*BoxA RNA. The *Ec*NusB-F122D spectrum with excess *Ec*BoxA (red contours) shows very small shifts from free *Ec*NusB-F122D (green contours) and does not exhibit the marked changes in the wild-type *Ec*NusB spectrum with *Ec*BoxA bound, shown in Supplementary Figure S3B. (**C**) Observed Δδ of NH resonances of free *Ec*NusB-Y18D from wt *Ec*NusB. In the native protein structure (22), Y18 makes NOE and H-bond contacts with Q79. The Y18D mutant protein indicates changes in these contacts based on the chemical shifts near residue Q79. (**D**) HSQC spectral overlay of free *Ec*NusB-Y18D (green contours) and a 1:1 complex of *Ec*NusB-Y18D with *Ec*BoxA (red contours). The *Ec*NusB-Y18D-BoxA spectrum is similar to the wt *Ec*NusB-BoxA spectrum shown in Supplementary Figure S3B.

SUPPLEMENTARY FIGURE S5

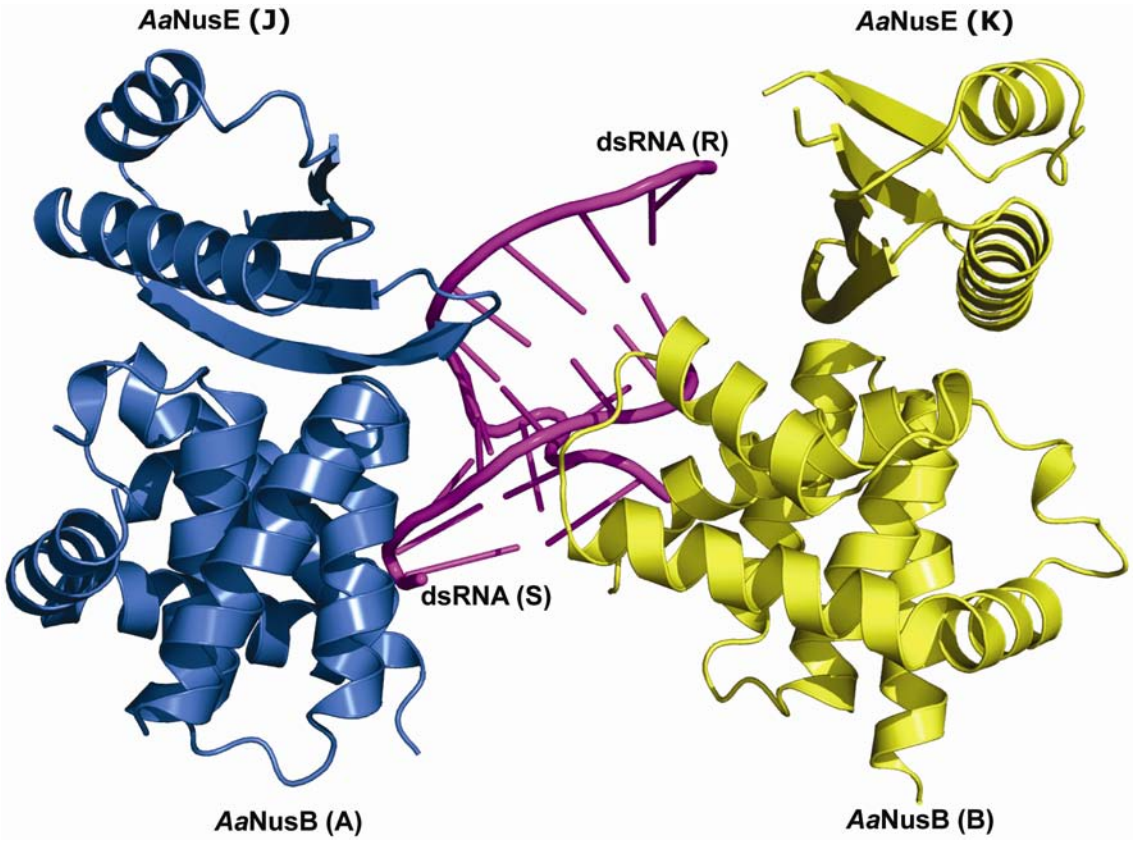

Figure S5. Overall structure of the asymmetric unit of *Aa*NusB-NusE-dsRNA. The structure reveals two copies of each macromolecule, in which two 12-mer RNA molecules form a pseudo duplex flanked by the two *Aa*NusB-NusE heterodimers on either side, each interacting in a slightly different manner. Chains A and J (blue) are believed to be biologically relevant with respect to dsRNA binding and were used in all analyses and discussions in the main text.

SUPPLEMENTARY FIGURE S6

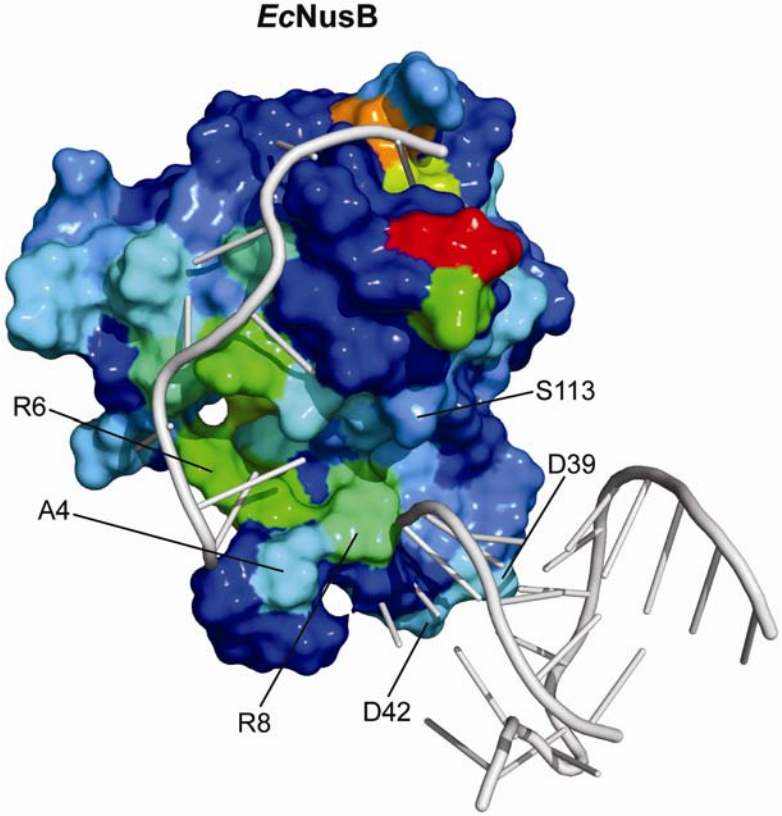

Figure S6. Implications for dsRNA binding by *Ec*NusB. Surface representation of the *Ec*NusB chemical shift map upon binding of an RNA consisting of *Ec*BoxA and *Ec*BoxB (tube-and-sticks in white), positioned as in the *Aa*NusB-NusE-BoxA and *Aa*NusB-NusE-dsRNA structures. The residues are colored according to the magnitude of Δδ (*Ec*NusB-BoxA subtracted from *Ec*NusB-BoxA-BoxB) ranging from ~0 ppm (blue) to 0.13 ppm (red). The region of *Ec*NusB that is highlighted by the shift map illustrates the contact surface for *Ec*BoxB, and is consistent with the dsRNA-binding site in the crystal structure of *Aa*NusB-NusE-dsRNA.

SUPPLEMENTARY FIGURE S7

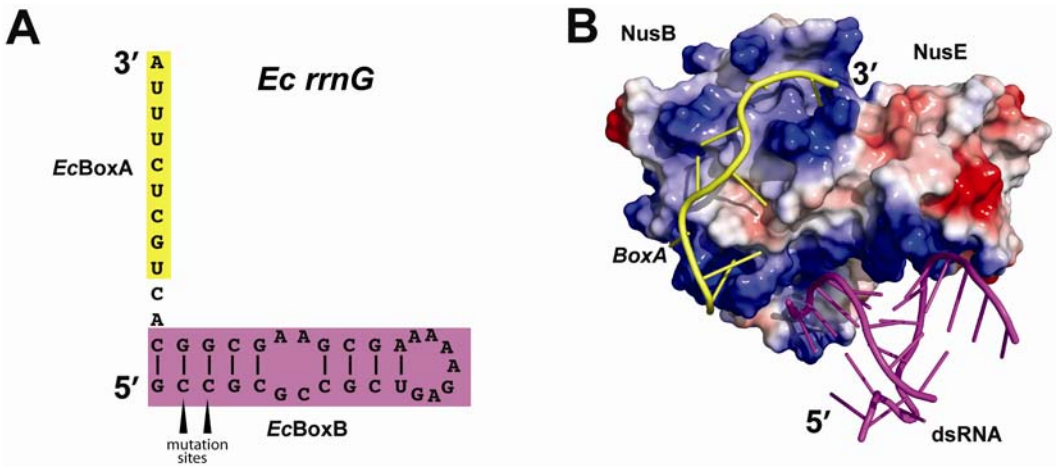

Figure S7. Implications for BoxA and BoxB binding to the NusB-NusE complex in *Ec rrnG* antitermination. (**A**) The sequence of *rrnG* RNA with BoxA highlighted in yellow and BoxB highlighted in magenta. (**B**) Superposition of the crystal structures of *Aa*NusB-NusE-BoxA and *Aa*NusB-NusE-dsRNA. This representation of the superimposed structures serves as a model for potential binding sites for BoxA and BoxB. The protein surface is colored by electrostatic potential (red, negative; blue, positive). Arrow heads in panel A indicate the single mutation sites that impair *rrnG* antitermination (19).